Numerical Analysis of GTAW Arc Behaviors in External Axial Magnetic Field

Xianqing YIN*, Yuanyi WU*, Jianxun ZHANG*, Ninshu MA and Jianjun GOU***
* School of Material Science and Engineering, Xi'an Jiaotong University, Xi'an 710049, China
** JWRI, Osaka University, Osaka 567-0047, Japan

KEY WORDS: (Welding Arc Behaviors), (External Axial Magnetic field), (Magneto Fluid Dynamics), (Numerical Analysis), (Experimental Validation)

1. Introduction

In welding process, it is widely accepted that grain refinement is an effective way to improve the properties of welding joints. When fine equiaxed grain was formed in the microstructure of welding joints, the tendency of welding crack would be decreased, and mechanical properties would be improved [1]. In seeing this, both metallurgical methods, by adding alloying elements in the welding pool, and mechanical methods, by mechanically stirring or vibrating the welding pool, have been broadly investigated to refine grains. In practice, a lot of methods, such as mechanical vibration [2-3], ultrasonic vibration [4-5], pulse current [6-7], electromagnetic stirring, has been implemented to stir or vibrate the welding pool and thus refine the grains. During all of such mechanical methods, electromagnetic stirring distinguished itself by its lower investment and applicability.

Generally, research on electromagnetic stirring welding concentrates on three aspects listed as arc behaviors, analysis of microstructure & properties, and model of welding arc & pool. In all of three concerns mentioned above, arc behaviors are so general and basic for understanding the mechanism of electromagnetic stirring, because arc behaviors are responsible for the heat transfer, heat distribution, penetration and vibration of weld pool. So, research on arc behaviors should be stressed and given a priority.

Many researchers have done a lot of work about welding arc and acquired many great achievements [8-14], even though it is a very long and hard journey. In present paper, MHD equations are built in order to describe the GTAW arc behavior at external constant axial magnetic field. With the help of CFD software FLUENT, the GTAW arc behaviors are studied and discussed. The arc pressure is measured and the results are used to validate the model.

2. Experimental system

Fig.1 shows the experimental system used in this work. We made an exciting coil, and a DC power provides the exciting current, and then the coil generates the axial magnetic field. The arc pressure is investigated by the data collecting card and the pressure sensor which is connected with the hole in the center of the water-cooled copper.

3. Mathematical model

Fig.2 is the calculation domain. Area 1 is the cathode tip, Area 2 is the anode surface, Area 3 is the side of anode, Area 4 is the bottom of anode, Area 5 is the gas inlet and Area 6 is the gas outlet. The domain is a cylinder with the radius of 10 mm and the height of 9 mm. The radius of cathode is 1.6 mm, the cone angle of cathode is 60^0. The cathode has a flat tip, and the arc length is 3 mm.

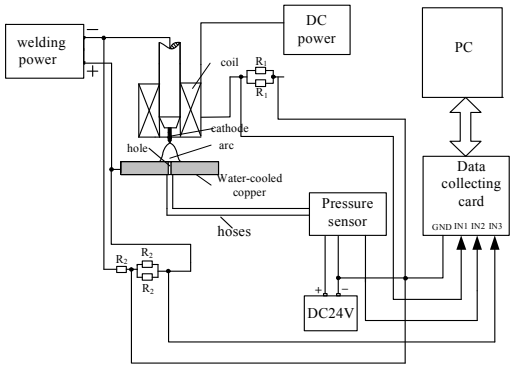

Fig.1 Experimental system

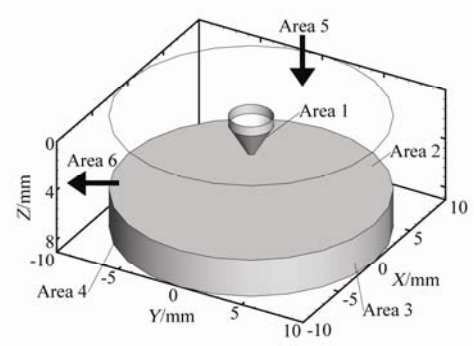

Fig.2 Calculation domain

Considering the characteristics of the plasma arc, following assumptions [15] have to been made:

(1) the plasma meets local thermodynamic equilibrium (LTE) condition, that means all the domain can be described by only one temperature;
(2) the flow is in steady-state;
(3) the plasma is optically thin;
(4) the gravity force and the viscous heating can be neglected.

These equations are based on CFD equations and Maxwell equations. The specific forms are following equations:

Table 1 Boundary Conditions

Boundary	*T*	*P*	*V*	*φ*	*A*
Area 1	3500K	$\frac{\partial p}{\partial x_i}=0$	0	$j=j_{\exp}$	$\frac{\partial A_i}{\partial x_i}=0$
Area 2	$q=q_c+q_e$	$\frac{\partial p}{\partial x_i}=0$	0	Coupled	$\frac{\partial A_i}{\partial x_i}=0$
Area 3	300K	–	–	$\frac{\partial \varphi}{\partial x_i}=0$	–
Area 4	1000K	–	–	0	–
Area 5	300K	1 atm	$Q_m=0.27\ g\ s^{-1}$	$\frac{\partial \varphi}{\partial x_i}=0$	0
Area 6	300K	1 atm	$\frac{\partial V}{\partial x_i}=0$	$\frac{\partial \varphi}{\partial x_i}=0$	0

Mass conservation:

$$div(\rho V)=0$$

Momentum:

$$div(\rho v_i V)=-div(\Gamma_v grad v_i)+S_v$$

Energy:

$$div(\rho h V)=-div(\Gamma_h grad h)+S_h$$

Electric potential:

$$div(\sigma grad\phi)=0$$

$$J=\sigma E$$

Magnetic potential:

$$div(gradA_i)=-\mu j_i$$

$$B=\nabla\times A$$

Turbulence kinetic energy:

$$div(\rho K V)=-div(\Gamma_K gradK)+G-\rho\varepsilon$$

Rate of dissipation:

$$div(\rho\varepsilon V)=div(\Gamma_\varepsilon grad\varepsilon)+\frac{\varepsilon}{K}(c_1 G-c_2\rho\varepsilon)$$

In these equations, V is the velocity, h is the enthalpy, ϕ is the electric potential, A is magnetic potential, μ_0 is the magnetic conductivity of vacuum, μ is the laminar viscosity, ρ is the density, K is the turbulence kinetic energy and ε is the rate of dissipation.

The inert gas is argon, and the thermodynamic and transport properties of argon are taken from document [16]. Boundary conditions adopted are summarized in table 1.

The current density on cathode surface is determined by:

$$\int_0^{R_c} 2\pi r j_{\max} dr+\int_0^{L} 2\pi r j(x) dl=I$$

, where R_c is the radius of hot area in front of cathode tip, and in this paper it equals to the radius of the tip. And j_{max} is the current density in the hot region, while j_i is that of other parts and it decrease from j_{max} to 0 along the cathode conical surface. The sum of these two parts of current is the welding current[17]. The welding current is 170 A in this work.

4. Results and discussion

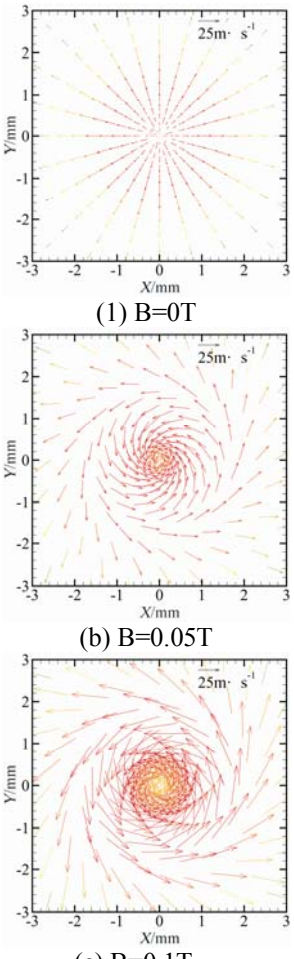

(1) B=0T

(b) B=0.05T

(c) B=0.1T

Fig.3 Velocity distribution of arc in the horizontal section (0.01mm above the anode surface)

When the arc is free, velocity vectors of the plasma are in the radial direction, like Fig.3 (a) shows. The plasma draws close to the axis because of the self-induction

magnetic field. However, when there is an external axial magnetic field, the arc will rotate and its velocity distribution showed in Fig.3 (b) and Fig.3 (c) will be like whirlpool. As a result of the arc rotation and centrifugal force, the plasma in arc center areas transfers to edge regions. And there comes a low plasma density area, and this sort of "hollow hole" enables the plasma at anode surface to flow back to the arc center area. This phenomenon is showed in Fig.4.

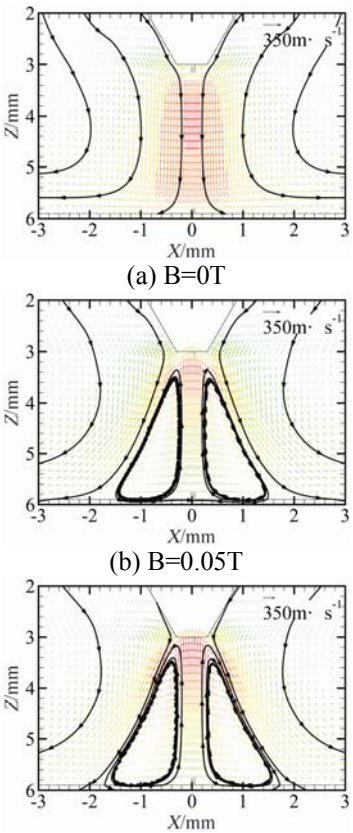

(a) B=0T

(b) B=0.05T

(c) B=0.1T

Fig. 4 Velocity distribution of arc in axial section

Fig.5 presents the comparison between the experimental and calculated arc pressure distribution along the radial direction at anode surface. A good agreement can be seen from the figures. In addition, the arc pressure distribution at anode surface turns from gauss distribution to double-peak one.

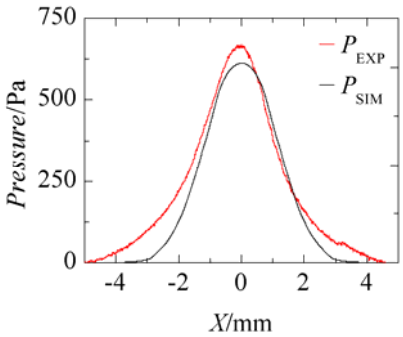

(a) B=0T

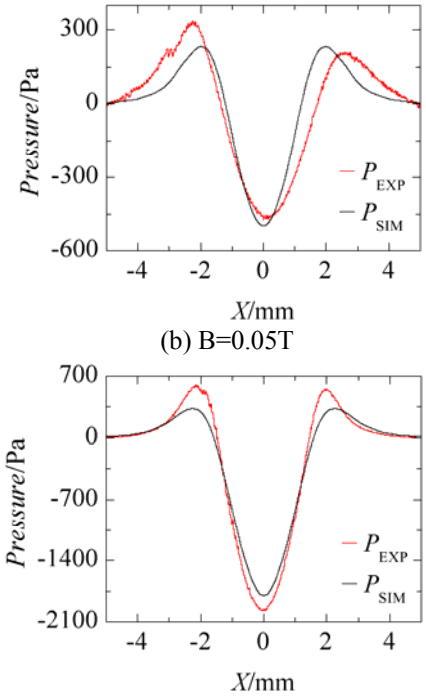

(b) B=0.05T

(c) B=0.1T

Fig.5 Pressure distribution of arc at anode surface: P_{EXP}-experimental results; P_{SIM}-simulated results.

In Fig.6, temperature distribution in the axial cross section is displayed. When the arc is free, the maximum temperature of the arc is 20400K and appears in front of the cathode tip. The center area has higher temperature than the border zone. In contrast, a low-temperature zone between the center high-temperature area and the anode surface can be seen if there is an external magnetic field. The temperature in this area is lower than border areas. And in this case, the arc becomes typical "Bell-type". This is because of the transportation of the plasma in the center area and the backflow of the plasma at anode surface.

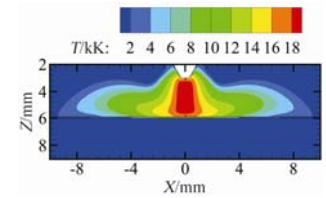

(a) B=0T

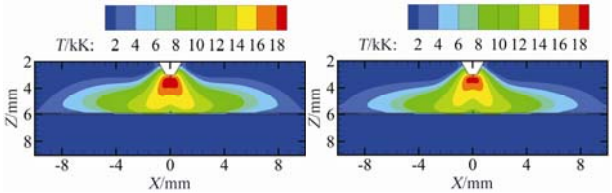

(b) B=0.05T (c) B=0.1T

Fig.6 Temperature distribution in the axial section

In Fig.7, we report the heat flux profiles on the anode surface. In external axial magnetic fields, the distribution of anode heat flux becomes double-peak. Generally speaking,

heat flux profiles towards the anode flatten out and the affected anode zone is bigger.

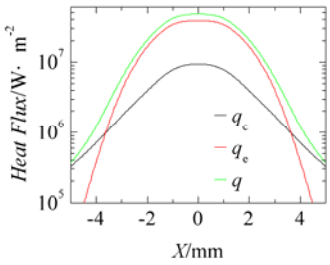

(a) B=0T

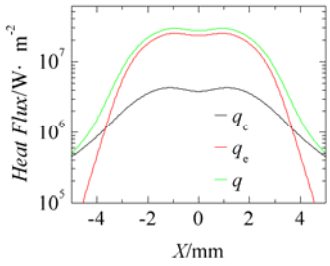

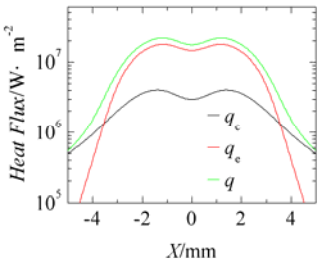

(b) B=0.05T (c) B=0.1T

Fig7. Heat flux of arc at anode surface

(q_r-radiation heat flux ; q_c-the heat due to conduction; q_e-charge motion.)

5. Conclusion

In present paper, GTAW arc in external axial field is analyzed. The arc behaviors have a lot of differences with the free arc ones, and the distributions of arc temperature, pressure and velocity have changed a lot.

Under the influence of external axial magnetic field, the arc becomes “Bell-type”. The arc rotates, the plasma in the arc center area transfers to edge regions and flows back, the high-temperature region has a contraction to the cathode, there is a low-temperature area under that region, the heat flux distributes as double-peak and the bottom arc extends, a zone of low or even negative pressure appears in arc center, the distribution of arc pressure in front of anode surface is double-peak.

References

[1] Kou S, Le Y. Nucleation mechanisms and grain refining of weld metal [J]. Welding Journal, 1986, 65 (12): 305-320.

[2] Qingguo Wang , Guofu Zhang , Jianjun Wang. Optimization of Vibration Welding Process Parameters with Low-frequency Mechanical Vibration [J]. Hot Working Technology, 2010, 39(3) : 141-143.

[3] Guofu Zhang, Tianmin Song, Chengjiang Yi, et al. The Effect of Mechanical Vibration Welding on the Microstructure of Weld and HAZ [J]. Transactions of the China Welding Institution, 2001, 22(3) : 85-87.

[4] Yangyang Fan, Qingjie Sun, et al. TIG welding of the stainless steel 304 based on the ultrasonic vibration [J] . Transactions of the China Welding Institution, 2008, 30(2) : 91-94.

[5] Watanabe T, Shiroki M, Yanagisawa A, et al. Improvement of mechanical properties of ferritic stainless steel weld metal by ultrasonic vibration [J]. Journal of Materials Processing Technology, 2010, 210 (12): 1646-1651.

[6] Balasubramanian M, Jayabalan V, Balasubramanian V. Effect of pulsed gas tungsten arc welding on corrosion behavior of Ti-6Al-4V titanium alloy [J]. Materials & Design, 2008, 29 (7): 1359-1363.

[7] Shengxi Wang, Gang Song, Liming Liu. Microstructure and property analysis of magnesium alloy welded with AC TIG welding and pulsed TIG welding [J] . Transactions of the China Welding Institution, 2006, 27(9) : 63-66.

[8] Ramakrishnan S, Stokes AD, Lowke JJ. An approximate model for high-current free-burning arcs. Journal of Physics D: Applied Physics, 1978, 11(16): 2267-2280.

[9] Hus KC, Etemadi K, Pfender E. Study of the free-burning high-intensity argon arc. Journal of Applied Physics, 1983, 54(3): 1293-1301.

[10] Freton P, Gonzalez JJ, Gleizes A. Comparison between a two- and a three-dimensional arc plasma configuration. Journal of Physics D: Applied Physics, 2000, 33(19): 2442-2452.

[11] Zhu PY, Lowke JJ, Morrow R. A unified theory of free burning arcs, cathode sheaths and cathodes. Journal of Physics D: Applied Physics, 1992, 25(8): 1221-1230.

[12] M.S. Benilov. Understanding and modelling plasma electrode interaction in high-pressure arc discharges: a review. Journal of Physics D: Applied Physics, 2008

[13] E Casado and V Colomer. The numerical modelling of Joule heating effects in thoriated tungsten cathodes of high-current plasma arcs. Journal of Physics D: Applied Physics, 2000

[14] Ma Q, Rong MZ, Wu Y, et al. Influence of copper vapor on low-voltage circuit breaker arc during stationary and moving states. Plasma Science and Technology, 2008. 10(3): 313-31

[15] Bini R, Monno M, Boulos MI. Numerical and experimental study of transferred arcs in argon. Journal of Physics D: Applied Physics, 2006, 39(15): 3253-3266.

[16] Murphy AB, Arundell CJ. Transport coefficients of argon, nitrogen, oxygen, argon-nitrogen, and argon-oxygen plasmas. Plasma Chemistry and Plasma Processing, 1994, 14(4): 451-490

[17] Tsai MC, Kou S. Heat transfer and fluid flow in welding arcs produced by sharpened and flat electrodes. Journal of Applied Physics, 1990, 33(10): 2089-2098